Received: 5 January 2022 | Revised: 19 September 2022 | Accepted: 26 October 2022 | Published on: 7 November 2022

DOI: 10.1002/joc.7908

RESEARCH ARTICLE

International Journal of Climatology RMetS

Increasing temperature extremes in New Zealand and their connection to synoptic circulation features

Anjali Thomas[1] | Adrian McDonald[1] | James Renwick[2] | Jordis S. Tradowsky[3,4] | Greg E. Bodeker[2,3] | Suzanne Rosier[5]

[1]School of Physical and Chemical Sciences, University of Canterbury, Christchurch, New Zealand

[2]School of Geography, Environment and Earth Science, Victoria University of Wellington, Wellington, New Zealand

[3]Bodeker Scientific, Alexandra, New Zealand

[4]Deutscher Wetterdienst, Regional Climate Office Potsdam, Stahnsdorf, Germany

[5]National Institute of Water Atmospheric Research (NIWA), Christchurch, New Zealand

Correspondence
Anjali Thomas, School of Physical and Chemical Sciences, University of Canterbury, Christchurch, New Zealand.
Email: anjali.thomas@pg.canterbury.ac.nz

Funding information
Ministry of Business, Innovation and Employment, Grant/Award Number: BSCIF1801

Abstract

Extreme temperature events (ETEs) have evolved alongside the warming climate over most parts of the world. This study provides a statistical quantification of how human influences have changed the frequencies of extreme temperatures in New Zealand, depending on the synoptic weather types. We use the ensembles under pre-industrial conditions (natural scenarios with no human-induced changes) and present-day conditions (anthropogenic scenarios) from the weather@home regional climate model. The ensemble simulations under these two scenarios are used to identify how human influences have impacted the frequency and intensity of extreme temperatures based on their connection to different large-scale circulation patterns derived using self-organizing maps (SOMs). Over New Zealand, an average two to three fold rise in frequencies of extremes occurs irrespective of seasons due to anthropogenic influence with a mean temperature increase close to 1°C. For some synoptic situations, the frequency of extremes are especially enhanced; in particular, for low-pressure centres to the northeast of New Zealand where the frequency of occurrence of daily temperature extremes has increased by a factor of 7 between anthropogenic and natural ensembles for the winter season, though these synoptic patterns rarely occur. For low-pressure centres to the northwest of New Zealand, we observe high temperatures frequently in both anthropogenic and natural ensembles which we expect is probably associated with warm air advection from the Tropics. The frequency of occurrence of high temperatures in these synoptic patterns has also increased by a factor of 2 between the natural and anthropogenic ensembles. For these synoptic states, the extremes are observed in the North Island and along the east coast of the country with the highest temperature along the Canterbury coast and Northland. The change between the natural and anthropogenic ensembles is largest on the west coast along the Southern Alps for all the synoptic circulation types.

Abbreviations: ETE, extreme temperature events; EWE, extreme weather events; GHGs, greenhouse gases; SOM, self-organizing map.

KEYWORDS
atmospheric circulation, attribution, climate change, extreme temperature, natural and anthropogenic scenario, New Zealand, self-organizing maps

1 | INTRODUCTION

The Intergovernmental Panel on Climate Change (IPCC) has frequently highlighted that, along with changes in the global mean surface temperature, the frequency and intensity of extreme weather events (EWE) has increased since the pre-industrial era (e.g., Masson-Delmotte *et al*., 2021). The rise in the concentrations of greenhouse gases (GHGs) in the atmosphere, which is driven primarily by human activities, is the main reason for the increasing frequencies and severity of EWEs (Masson-Delmotte *et al*., 2021). Anthropogenic increase in GHG concentration from 1951 can explain more than half of the observed increase in surface temperature according to Masson-Delmotte *et al*. (2021), Bindoff *et al*. (2013) and Hegerl *et al*. (2007) and with every degree of warming, unprecedented extreme events are to be expected (Fischer and Knutti, 2015). This change in both the severity and frequency of EWEs has been observed recently (Philip *et al*., 2021) and it impacts people and the economy in various ways, hence it is necessary to understand and estimate the impact of anthropogenic warming on such extremes (Douris and Kim, 2021). Within New Zealand extreme event attribution and the economic risks associated with EWEs is an active area of research (Frame *et al*., 2020; Stone *et al*., 2021; Tradowsky *et al*., 2022).

As the atmosphere warms, the distribution of temperatures shifts towards positive anomalies, leading to more frequent hot days and fewer cold extremes. Each EWE arises via a complex interaction of natural and anthropogenic factors. The special report on global warming of 1.5°C by the IPCC (Masson-Delmotte *et al*., 2018) examined various attribution analyses and concluded that the estimated anthropogenic global warming signal simulated under elevated anthropogenic GHG concentrations correlates with the observed warming. Hence, attribution studies need to be carried out to understand the influence of anthropogenic forcings and to predict the response of the climate system with respect to further increasing GHGs.

New Zealand had a cooler climate in the 19th century (Salinger *et al*., 1996), but global warming has caused a rise in surface temperatures, leading to trends in climate extremes (Salinger and Griffiths, 2001). Studies by Folland and Salinger (1995), Manton *et al*. (2001) and Salinger and Griffiths (2001) all noted significant increasing trend in temperatures for the South Pacific regions and that these trends were linked to changes in synoptic circulations and regional warming. Mullan (2012), Caloiero (2017) and Salinger *et al*. (2020a) also noted a linear warming trend over New Zealand and a significant contribution towards this warming was attributed to anthropogenic rise in GHGs (Dean and Stott, 2009). Evidence of anthropogenic forcings on 2013 New Zealand drought event was detected by Harrington *et al*. (2014).

Changes in synoptic-scale circulation patterns also influence the nature of weather systems and affect extreme events (Horton *et al*., 2015). Most of the key meteorological variables such as temperature, wind and precipitation are strongly influenced by these circulation patterns. Circulation changes in the late 1940s and the mid-1970s associated with an increase in temperature in New Zealand were detected by Salinger and Mullan (1999). Research by Horton *et al*. (2015) identified that it is likely that anthropogenic influences have altered these circulation patterns and their frequency of occurrence. Hence trends in extreme temperatures have been related to atmospheric circulation changes over the 1979–2013 period according to Horton *et al*. (2015). For example, in most of the extreme heat events around the globe, there is one common feature in their composition, that is, a high-pressure synoptic system. Typically, such a system is known as a "blocking high" and is a stationary system with a centre of high pressure that remains in the same location for a longer period of time and at a higher latitude than normal (Perkins, 2015). Blocking patterns are often associated with subsidence of air (high surface pressure), clear skies and associated warming (Horton *et al*., 2016). These types of persistent highs have been responsible for numerous heatwaves over Australia (Marshall *et al*., 2014).

Locations of these synoptic circulation types or the high- and low-pressure systems around New Zealand also influences temperature and precipitation events as they steer the direction of airflow onto the landmass (Figure 1). The influence of southerly and northerly flow variability on the temperatures of New Zealand has long been recognized (e.g., Trenberth, 1976). In particular, cold southerly or warm northerly air flow associated with different circulation types, in turn, affect precipitation patterns (Prince *et al*., 2021), glacial properties like ablation (Hay and Fitzharris, 1988) and can even impact pollution events as noted by Fiddes *et al*. (2016). Hence the locations of these

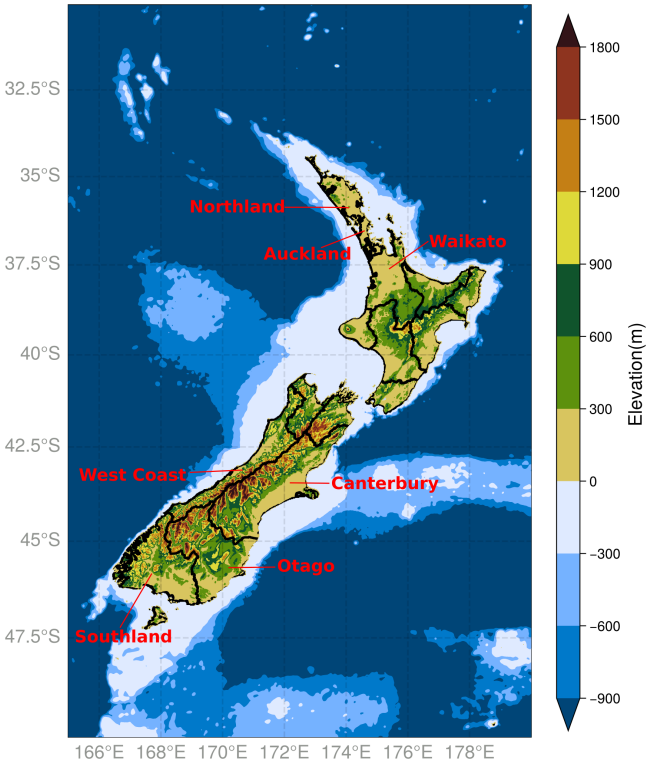

FIGURE 1 Topographical map of New Zealand constructed using the ETOPO1 Global Relief Model data with regions marked (Amante and Eakins, 2009) [Colour figure can be viewed at wileyonlinelibrary.com]

circulation patterns and their influence in controlling the airflow to the landmass are also important while studying extremes. Several classifications associated with circulation types over New Zealand have been carried out and the following ones represent those most widely used classifications. Trenberth defined weather regimes based on the pressure level indices (Trenberth, 1976) followed by Kidson, who classified the main synoptic circulation types over New Zealand into 12 major types (Kidson, 2000). Jiang later on derived 12 clusters of synoptic patterns using *K*-means clustering (Jiang, 2011).

Understanding the connection between specific circulation patterns and extreme temperatures and estimating their variation in scenarios with and without anthropogenic influences can provide an important attribution context for the occurrences of EWEs over New Zealand. The present study focuses on identifying and quantifying the frequency of occurrence, as well as the intensity, of extreme temperatures in scenarios representative of both natural pre-industrial conditions (also known as counterfactual or natural condition [NAT] with no human-induced changes) and present-day conditions (also known as factual or anthropogenically forced simulations [ANT]) from the weather@home regional climate model (Massey *et al.*, 2015; Black *et al.*, 2016). Ensembles under these two conditions are used to identify statistically whether increases in anthropogenic influence have impacted the likelihood and intensity of extreme temperatures and the extent to which these changes can be ascribed to the different large-scale circulation patterns occurring over New Zealand. We use a clustering method called the self-organizing maps (SOMs) (Kohonen, 2001) to identify the representative circulation features over New Zealand. We examine the probability distributions and spatial variability of daily maximum ($T_{\max}$) and daily minimum ($T_{\min}$) temperatures over New Zealand associated with each synoptic pattern. Extreme temperatures are calculated based on the percentile threshold values which are detailed in the coming sections. Finally, we composite the circulation patterns associated with more frequent extreme temperatures to understand how the intensity and frequency are affected at various regions around New Zealand and how circulation patterns contribute to the frequency of temperature extremes.

2 | DATA AND METHODOLOGY

2.1 | Datasets

In this study, we use two sets of data for the analysis. Mean sea level pressure (MSLP) data from both ERA5 (Hersbach *et al.*, 2020) and weather@home (w@h) (Massey *et al.*, 2015) datasets are used to generate synoptic circulation patterns using the SOM clustering technique. The gridded ERA5 reanalysis succeeds the ERA-Interim reanalysis (Dee *et al.*, 2011). Forty-one years (1979–2019) of MSLP data from ERA5 (0.25° × 0.25° resolution) were interpolated and resampled to the resolution of w@h (0.44° × 0.44° resolution), such that they could together be used for training the SOM algorithm.

Weather@home (Massey *et al.*, 2015) is a regional climate modelling system which runs as part of "climateprediction.net" (Allen, 1999). This distributed computing project harnesses the spare computing power donated by volunteers worldwide, enabling the creation of extremely large ensembles of simulations (order several thousands of members). In w@h, the UK Met Office global model HadAM3P (Pope *et al.*, 2000) is run with the regional model HadRM3P (Jones *et al.*, 2004) embedded within it. In the Australia-New Zealand region—w@h ANZ (Black *et al.*, 2016), w@h is configured to run over the CORDEX Australasian domain (Evans, 2011).

The atmosphere-only global and regional models are based on the atmospheric component of the UK Met Office Hadley Centre Climate Model HadCM3 (Gordon *et al.*, 2000) and need to be supplied with sea surface

temperatures and sea ice fraction at their lower boundary. Here, these were taken from the UK Met Office Operational Sea Surface Temperature and Sea Ice Analysis (OSTIA) dataset (Donlon *et al.*, 2012). In addition, the models were supplied with values of well-mixed GHGs (CO_2, CH_4 and N_2O), ozone, aerosols, halocarbons and sulphur species; in this case, these were prescribed to follow those used in the Coupled Model Intercomparison Project 5 (CMIP5; Taylor *et al.*, 2012), with the RCP8.5 emissions scenario followed after 2005 for GHGs and aerosols.

In order to quantify the effects of anthropogenic influence, a so-called "natural" (NAT) or "counterfactual" set of simulations was created, which models "the climate that might have been" in the absence of anthropogenic influence. For these NAT simulations, values of the atmospheric composition were set to pre-industrial values and several estimates of the naturalized SST forcing were supplied. NAT SSTs were computed by taking the attributable warming patterns in SST from CMIP5 global coupled models, plus a multimodel mean, and subtracting them from the OSTIA present-day fields; in this way an attempt is made to span the inherent uncertainty in the counterfactual SST state.

Very large ensembles of simulations of the anthropogenic (ANT) and natural (NAT) worlds were created by introducing a small perturbation into the initial conditions of each model simulation, representing the chaotic "noise" inherent in the climate system and enabling an estimate of the range of possible climate and weather states. As described by Black *et al.* (2016), 1,740 perturbations were applied, but these can be applied to various initial condition states, enabling the creation of any number of realizations. The natural climate forcings, volcanic aerosol and changes in solar irradiance, were common to both, and there was no change in the land surface types between the two sets of simulations. Here, we used 2,908 ANT and 2,916 NAT simulations of the year 2014 (actually December 2013 through to November 2014). While not a multiyear climatology, the large ensembles do enable inferences to be made about anthropogenic influence on climate as these thousands of ensemble members are designed to represent the range of internal variability (Black *et al.*, 2016). We are doing a model-to-model (ANT and NAT) comparison in this study using w@h temperatures and our entire analysis has been completed over the temperature anomaly fields such that any biases in the model ensembles are avoided.

2.2 | Self-organizing map

Self-organizing maps (SOMs), also known as Kohonen maps, are a form of artificial neural network that performs unsupervised clustering of data (Kohonen, 2001). SOMs are similar to traditional cluster classification methods such as *k*-means clustering, but tend to classify events more uniformly and provide a mechanism to visualize the complex distribution of synoptic states while treating data as a continuum (Hewitson and Crane, 2002). SOMs generate patterns using an unsupervised neural network trained with a competitive learning algorithm such that it adjusts a set of reference vectors or nodes on the basis of differences between the reference vector and each input field. Node weights are adjusted based on their proximity to "winning" nodes (i.e., nodes that most closely resemble a sample input). Training over many iterations of input datasets results in grouping similar patterns together and keeping dissimilar ones separate.

The first step of the SOM algorithm is to present a random subsample set from the whole data to initialize the SOM. This random initialization generates a set of nodes which act as the reference vectors. Later, as new fields are presented to the SOM, the similarity between the input data and the reference vector nodes is calculated. Identifying the best matching unit (BMU) is completed by running through all reference vectors and calculating the Euclidean distance from each input data vector to the reference vector. The shortest distance between the reference vector and the input vector is the winning node and is labelled as the BMU. While there are numerous ways to determine the distance, however, the most commonly used method is the Euclidean distance (d), which is also the distance metric used in this study,

$$d = \arg\min\{|x - m_i|\},$$

where x is the input vector which is compared with a set of i reference nodes m_i to identify the BMU which then gets modified along with its neighbour nodes. The learning rate determines how this adjustment is related to the difference between the reference vector and the input data and is defined within the SOM setup. During the training iterations the best matching vector and its neighbours are updated using the algorithm,

$$m_i(t+1) = m_i(t) + hd_i(t)[x(t) - m_i(t)],$$

where t is the step index and $hd_i(t)$ is the neighbourhood function of the kernel given by

$$hd_i(t) = \alpha(t)\exp\left(\frac{(|r_d - r_i|)^2}{2\sigma^2(t)}\right),$$

where $\alpha(t)$ is the learning rate which decreases with time in the range [0,1], $\sigma(t)$ is the width of the neighbourhood

function which determines the range of the neighbour nodes examined when updating the vectors, and r_d and r_i are the radius vectors for reference vectors d and i. The iteration process continues through several cycles until there is no further modification of the neighbour nodes. Thus, the SOM nodes are adjusted for all the iterations along all the input data until convergence is acquired. Thus, the resultant map will have neatly distributed and organized patterns in the data space with an expectation of a very small average quantization error. The quantization error is the average of all the minimum Euclidean distances.

Many methodological choices must be made before defining a SOM. For the input data, we choose to use 41 years of MSLP data (1979–2019) from ERA5, and randomly pick 41 simulation years from each of thousands of w@h ANT, and w@h NAT simulations, to train the SOM. Here both the reanalysis dataset and w@h factual and counterfactual simulations are used to incorporate realism into the circulation patterns obtained from the SOM. Training the SOMs on both ERA5 and weather@home datasets results in a more robust training that benefits from ERA5 being a good representation of real-world variability and the large ensemble size of the w@h data that can also produce patterns of variability that, while realistic, may not have been observed in the historical ERA5 record. This is very similar to the methodology used by Mason *et al.* (2015) and McDonald *et al.* (2016). This is the initial step along with the number of nodes being defined by the user.

Different sets of SOMs, with different node configurations, are tested to find the optimal SOM parameters, such as the learning rate and the width of the kernel which influences the modification of neighbouring nodes, such that the quantization error is minimized (McDonald *et al.*, 2016). The choice of the number of the SOM nodes is also partially defined by how detailed the representative synoptic patterns should be as each node represents a circulation type. Too many nodes/synoptic patterns will be impractical to separate and distinguish between each other, whereas too few nodes may not be able to represent all the changes in the synoptic state and will be too general (Loikith *et al.*, 2017).

Various numbers of nodes were examined ranging from 10 to 30 nodes and pattern correlations were analysed to define the ideal size of the SOM. After quantitatively and qualitatively assessing the results obtained from the smaller and the larger node numbers, we concluded that a (12 nodes) configuration captured the range of synoptic circulation features and variability well and was compact enough to allow physical interpretation. Given that the SOM mapping places similar nodes together, it can be seen in Figure 2a that there is a well-defined pressure gradient that develops across the SOM nodes from top left to bottom right. All the pressure patterns are also unique and distinguishable. All the dominant high-pressure systems (anticyclones) are grouped towards the top left corner of the figure while all the nodes representing low-pressure circulation patterns are aligned at the bottom right area and the moderate pressure types on the diagonal between these two extremes (Figure 2a). Many synoptic patterns observed here are similar to the Kidson synoptic types described in Kidson (2000), which are trough patterns (low pressure over and east of the country) (similar to nodes 3, 6, 12), zonal types (intense anticyclones north of 40°S and strong westerlies to the south of the country) (nodes 5, 9) and blocking patterns (high centres lying to the south and east of the analysis region; nodes 1, 4). Kidson's types are referred to here due to the similarity of patterns even though using these synoptic classification types in a general circulation models (GCM) outputs over New Zealand is not effective. Prior work by Parsons *et al.* (2014) states that Kidson's types is not identified to be sensitive enough to relate subtle regional climate change signals in the model due to the model uncertainty.

The pressure anomaly in Figure 2b shows how well the pressure patterns are arranged around New Zealand. The positions of pressure patterns change around the landmass in a continuous manner as we move from one node to another. Low-pressure centres shift from west to east of the landmass as we move from left to right. To ascertain the robustness of the appropriate SOM node selected, the pattern correlation between the different synoptic systems represented by each node in the SOM and all the data for each day assigned to that node was analysed for both the ANT and NAT ensemble simulations. Days with circulation patterns similar to each SOM node are identified using the Euclidean distance and then clustered together for the correlation calculation. The methodology used here is similar to that in Gibson *et al.* (2016) and McDonald and Parsons (2018). Figure 3 shows the distribution of the Pearson correlation coefficients for each node, which demonstrates the quality of the SOM classification. The mean correlation value for all the nodes is above 0.5 which is a good indicator that each node in the SOM is representative of its members. As the pressure values do not show much variability in the anthropogenic atmosphere, the correlation patterns for both ANT and NAT are very similar (not shown).

To visualize the relationship between the SOM nodes, we also create a Sammon map (Sammon, 1969) from the SOM output. Sammon maps take the higher dimensional SOM representation, and use statistical relations between each SOM node and its neighbours, and projects that information onto a two-dimensional space. A Sammon map for our SOM is shown in Figure 4. The Euclidean distances are calculated between different SOM nodes

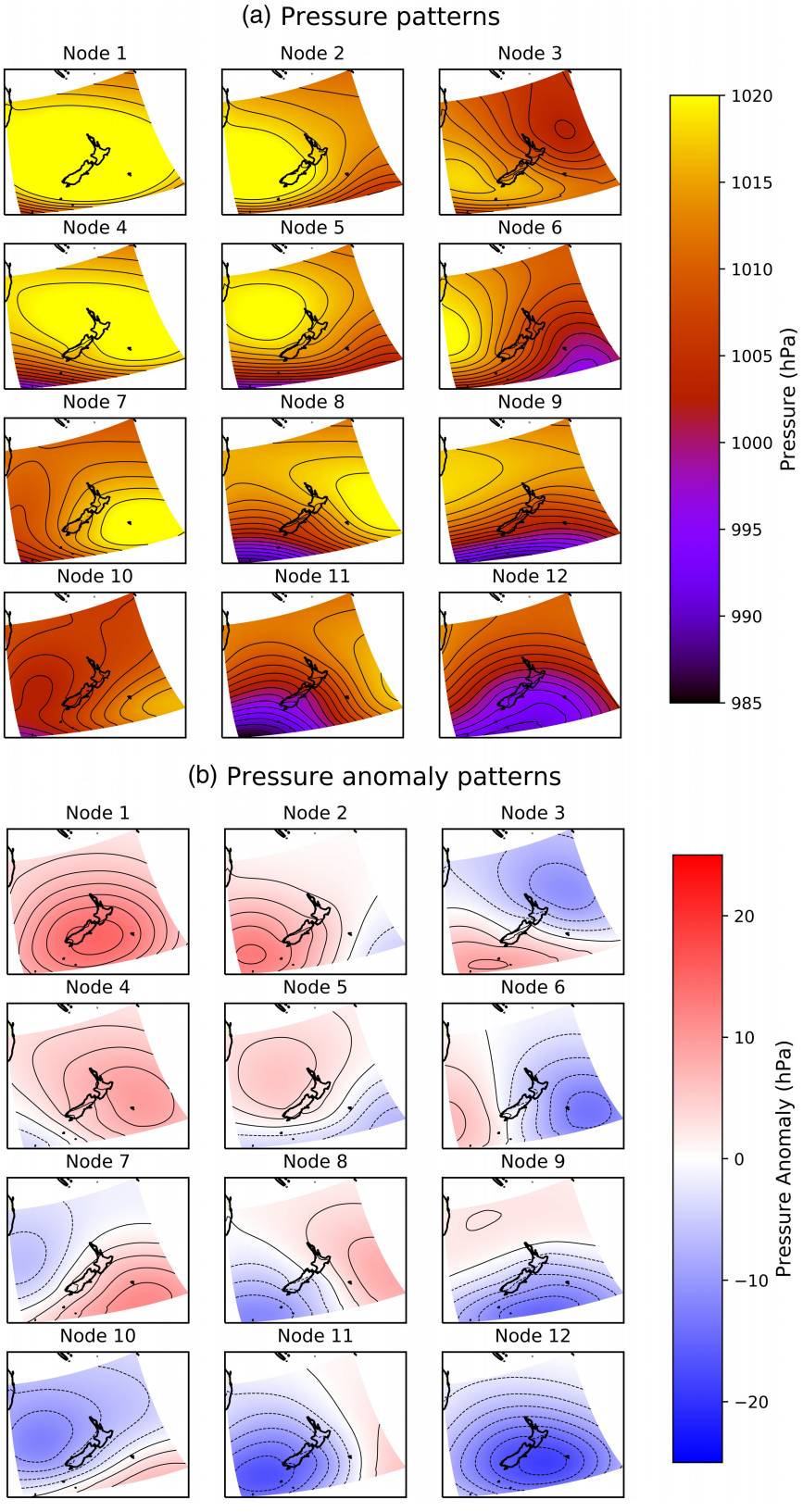

FIGURE 2 (a) 4 × 3 SOM (12 nodes) derived from w@h MSLP fields and ERA5 MSLP fields over the New Zealand domain. (b) Same specifications as that of (a) but the anomaly pressure patterns. The climatology used to calculate the anomaly is the average of all the data that goes into training the SOM, that is, ANT, NAT and ERA5 datasets. Node 1 corresponds to the top left pattern (high pressure) and node 12 to the bottom right (low pressure) [Colour figure can be viewed at wileyonlinelibrary.com]

and are reduced to a less complex two-dimensional array which is easily visualized and interpreted. The Sammon map provides a clear idea of the position of each node relative to every other node so that we can potentially group similar nodes into larger clusters within our SOM. For example, nodes 3 and 6 are closer and more similar to each other than any other nodes forming a cluster within the SOM. We also see that the Sammon map represents a

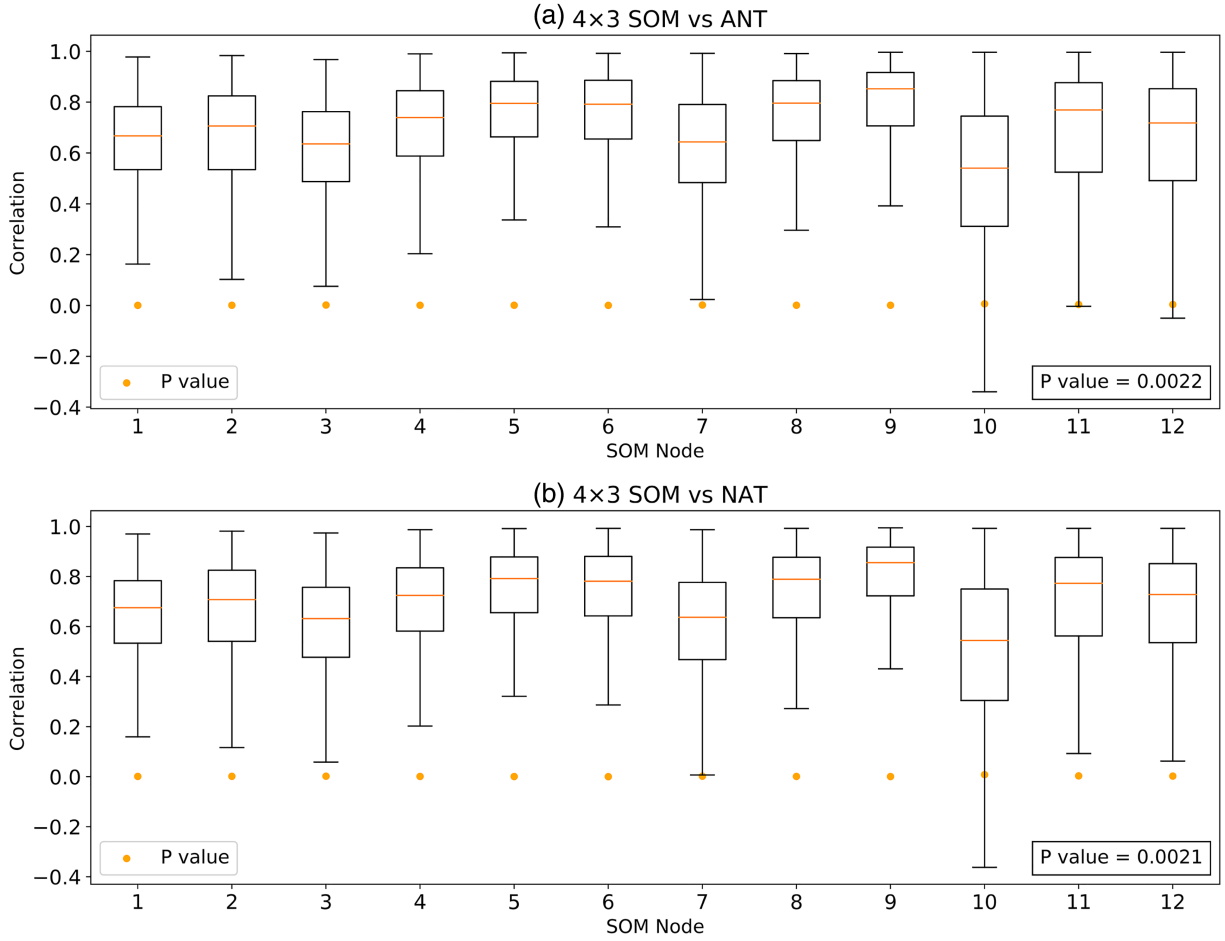

FIGURE 3 Boxplots of Pearson pattern correlation coefficients between the 12 circulation patterns in the SOM and (a) ANT w@h ensemble simulation which match best with each node using the Euclidean distance measurement (b) similar to (a) but for NAT w@h ensembles. *p*-values quantify the statistical significance of the correlation test. If the *p*-value is lower than .05, then there is a significant correlation between the variables [Colour figure can be viewed at wileyonlinelibrary.com]

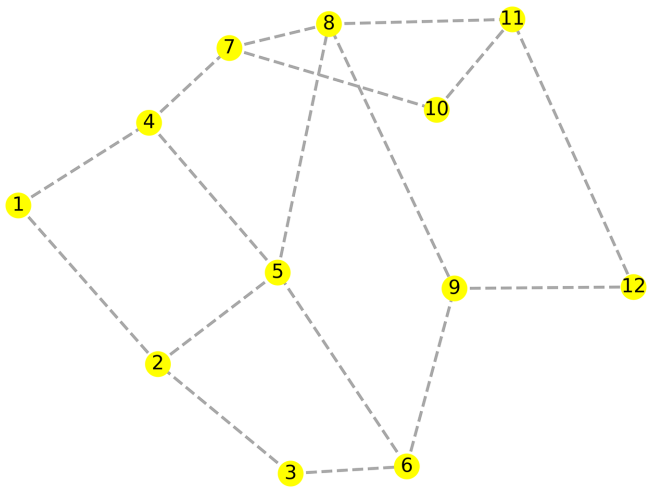

FIGURE 4 Sammon map for the 4 × 3 SOM (Figure 2). The numbers indicate each node in the SOM and they are positioned in the plane relative to its similarity with the neighbour nodes [Colour figure can be viewed at wileyonlinelibrary.com]

relatively uniform grid which is a sign of a well-functioning classification.

Climate extreme indices defined by the Expert Team on Climate Change Detection and Indices (ETCCDI) (Zhang *et al.*, 2011) (www.wcrp-climate.org/etccdi) are used to examine the temperature variation between the two forcings—ANT and NAT. Two percentile-based indices TX90p (percentage of days when $(T_{max}) > 90$th percentile, also known as percentage of warm days) and TN90p (percentage of days when $(T_{min}) > 90$th percentile or percentage of warm nights) are used in this study. Extreme temperatures associated with SOM nodes are also computed in the later analysis, where extreme temperatures are determined using a threshold of 90th percentile of NAT simulations. The frequency analysis is based on area averaged (land points over New Zealand) 90th percentile values, whereas for spatial analysis the ensemble simulations are averaged at each grid point.

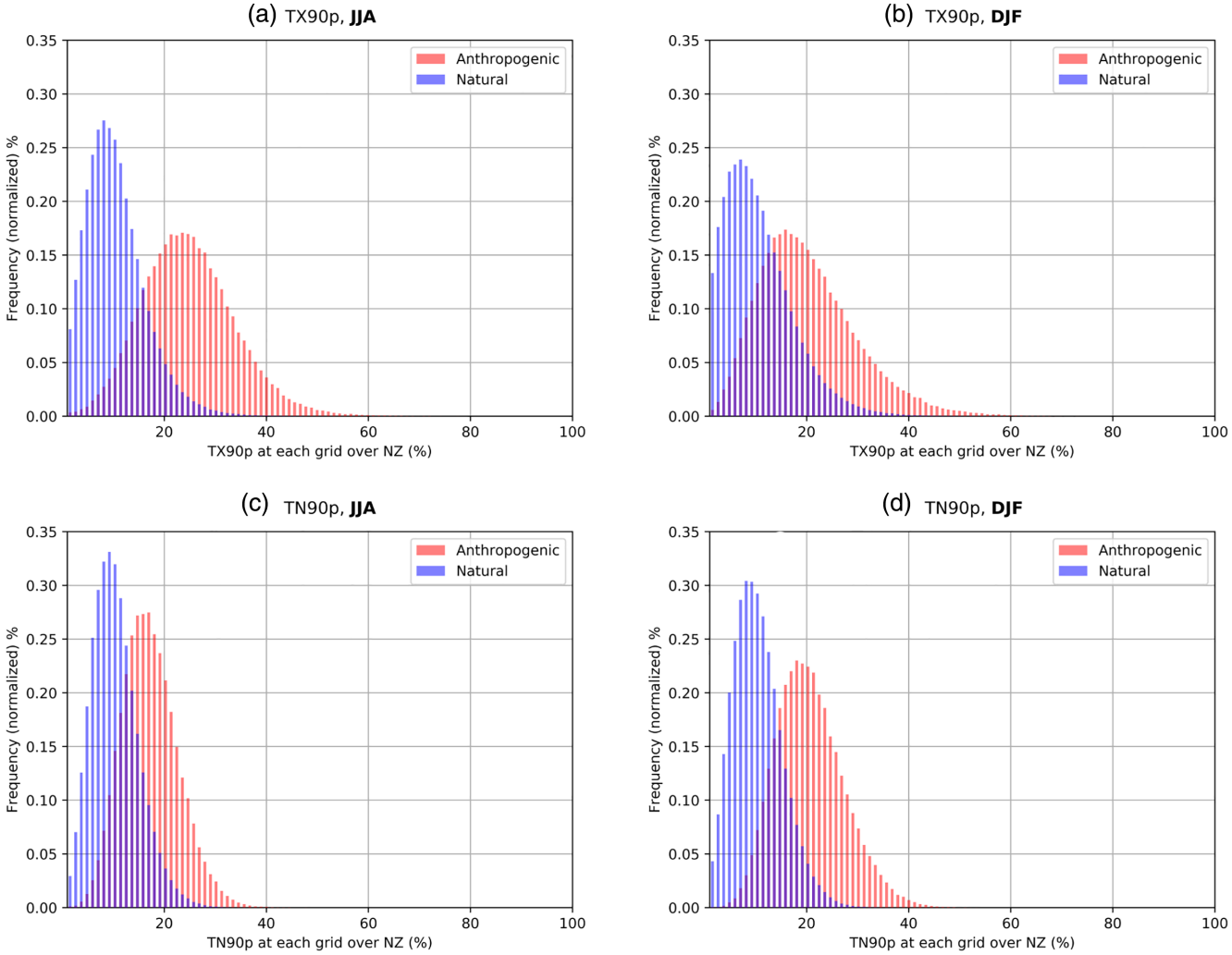

FIGURE 5 Probability distribution of percentile-based temperature extremes indices from ETCCDI for w@h ANT and NAT model ensembles (a) TX90p for JJA, (b) TX90p for DJF, (c) TN90p for JJA, (d) TN90p for DJF. The baseline (90th percentiles values) used for calculating the indices are the 90th percentiles from the NAT ensembles [Colour figure can be viewed at wileyonlinelibrary.com]

3 | RESULTS AND ANALYSIS

3.1 | Temperature distribution

The distribution of some of the climate extremes indices defined by the ETCCDI are analysed to provide an initial insight into how temperatures vary for the different ensembles and seasons. We use percentile-based threshold indices which identify the exceedance rate above the 90th percentile (90p) for daily maximum temperatures (denoted as TX90p also known as percentage of warm days) and daily minimum temperature (TN90p or percentage of warm nights). All the simulations from the NAT ensemble are used to determine the 90th percentile threshold, based on which TX90p and TN90p are calculated. TX90p is the percentage of maximum temperature ($T_{\max}$) above the 90th percentile for each simulated year and TN90p is the percentage of minimum temperatures ($T_{\min}$) above the 90th percentile which is the warm nights for each simulated year. The distributions of TX90p and TN90p are shown in Figure 5 for the Southern Hemisphere winter (JJA) and summer (DJF). Since we use the 90th percentile of NAT simulations as the threshold, the TX90p and TN90p indices are always 10% for the NAT ensemble as seen in the figures (Figure 5). It is clearly observed that the anthropogenic ensemble has a higher occurrence of extreme warm days than the natural ensembles in both seasons. The extremes in the pre-industrial scenario occur only due to natural variability whereas both natural variability and changes due to anthropogenic signals contribute towards the extremes in the ANT world which explains the higher occurrence of the percentage of warm days in the ANT ensemble. The winter season (JJA) TX90p shows the largest differences

between the two ensembles, with ANT experiencing warm days up to 25% of the time while individual years from the NAT ensembles have only 9–10% (Figure 5), which can be observed from the peaks of the distribution. Thus, on average extreme warm temperatures, as defined by the exceedance of the 90th percentile within the NAT ensemble, occur more than twice as often in the ANT than the NAT.

To understand how the maximum and minimum temperature extremes vary in frequency and intensity in relation to different circulation types, we group the days with the same circulation types together based on the SOM patterns identified in Figure 2. The MSLP circulation patterns and the associated extreme daily temperatures (T_{max} and T_{min}) for all the simulations of both ANT and NAT ensembles from the w@h model output are examined. The low-pressure systems are generally associated with cloudy and wetter weather conditions, typically with lower temperatures than usual, whereas high-pressure systems will often have dry and clear skies with a larger solar insolation at the surface leading to higher temperatures and larger diurnal variations. The large-scale synoptic pressure patterns also contribute to modulating temperatures by advecting air masses from either the equatorial belt or from the south. The temperatures associated with these synoptic circulation types will also vary with seasons causing intraseasonal variability (Kidson, 2000). In this study, our analysis is carried out in winter (JJA) and the summer (DJF) where there is a seasonal temperature change of 9–10°C and variation due to latitude from 14 to 9°C as we move from the North Island to the South Island. The other two seasons, autumn and spring, have moderately milder temperatures across the country and are not detailed for brevity.

The temperature anomalies are calculated relative to the climatology of all simulations in each ensemble and then the distributions are computed by mapping all daily fields to the appropriate SOM node using the Euclidean distance metric. As we are separating the temperature variables according to seasons, the mean and anomalies are different corresponding to the season. The probability density functions (PDFs) of the daily temperature anomalies for each circulation pattern (Figure 6) clearly identifies that anthropogenic forcing causes higher temperatures in all the synoptic weather regimes (all the 12 nodes from Figure 2a) irrespective of the seasons JJA (Figure 6a,b) and DJF (Figure 6c,d). Certain nodes like 4, 7, 8, 10 and 11 which are associated with low-pressure to the west of the country and which are related to a meridional flow (see Figure 2a) tend to be associated with positive anomalies. Both the spatially and ensemble averaged mean temperatures anomalies associated with each node/circulation type are higher in the anthropogenic ensemble than the natural ensemble. The tail of the PDF which represents the rarer temperatures will be investigated later, but is also clearly shifted to higher temperatures and higher occurrence rates.

If we consider the percentage occurrence of the synoptic weather patterns for each day (percentage of days mapped to each node which is same as the percentage frequency of occurrence of T_{max} and T_{min}; numbers inset each node in Figure 6) the largest variations in the frequencies of occurrence between the different synoptic types for both ANT and NAT are observed in the summer season (Figure 6c,d), especially in the left column (nodes 1, 4, 7 and 10). The winter season (Figure 6a,b) has more uniform occurrences across different synoptic patterns. The differences in the frequency of occurrences of T_{max} and T_{min} in the anthropogenic simulations ANT and natural simulations NAT for each synoptic type are examined. In winter, nodes 3, 10 and 12 show the most decline whereas in summer it is nodes 6, 9 and 12 (see Figure 2a). This decline of trough-like synoptic patterns in the ANT ensemble, when compared with NAT, is most prominent in the summer season. Previous work detailed in Sturman and Quénol (2013) and Jiang *et al.* (2013) also reported that trough weather systems which are related to enhanced cloud development have declined in frequency, while the zonal (anticyclones north of 40°S and westerly flow to the south of the country) and anticyclones (dominant high-pressure systems) have increased in occurrence over New Zealand (Sturman and Quénol, 2013). The corroboration of this result using the w@h ensembles gives us some confidence in the predictive power of these simulations.

To further focus our analysis on the extreme temperature, the exceedance of the minimum and maximum temperature above a certain threshold is assessed. In this way the frequency of occurrence of these extremes can be quantified, in connection to each category of the weather patterns in the SOM. Following the analysis of the temperature anomaly PDFs in Figure 6, we focus on the extremes which fall in the high tail of the distribution curves for daily maximum (T) and minimum (T_{min}) temperatures. Figure 7 represents the distribution of temperature anomalies above the 90th percentile value of the NAT for the two ensembles (ANT and NAT) over the New Zealand domain for both winter (Figure 7a,b) and summer (Figure 7c,d). The percentage frequency of occurrence associated with each SOM node is calculated and displayed in each panel. The frequency of occurrence is the count of total days associated with each node divided by the count of total days in the respective ANT and NAT ensemble.

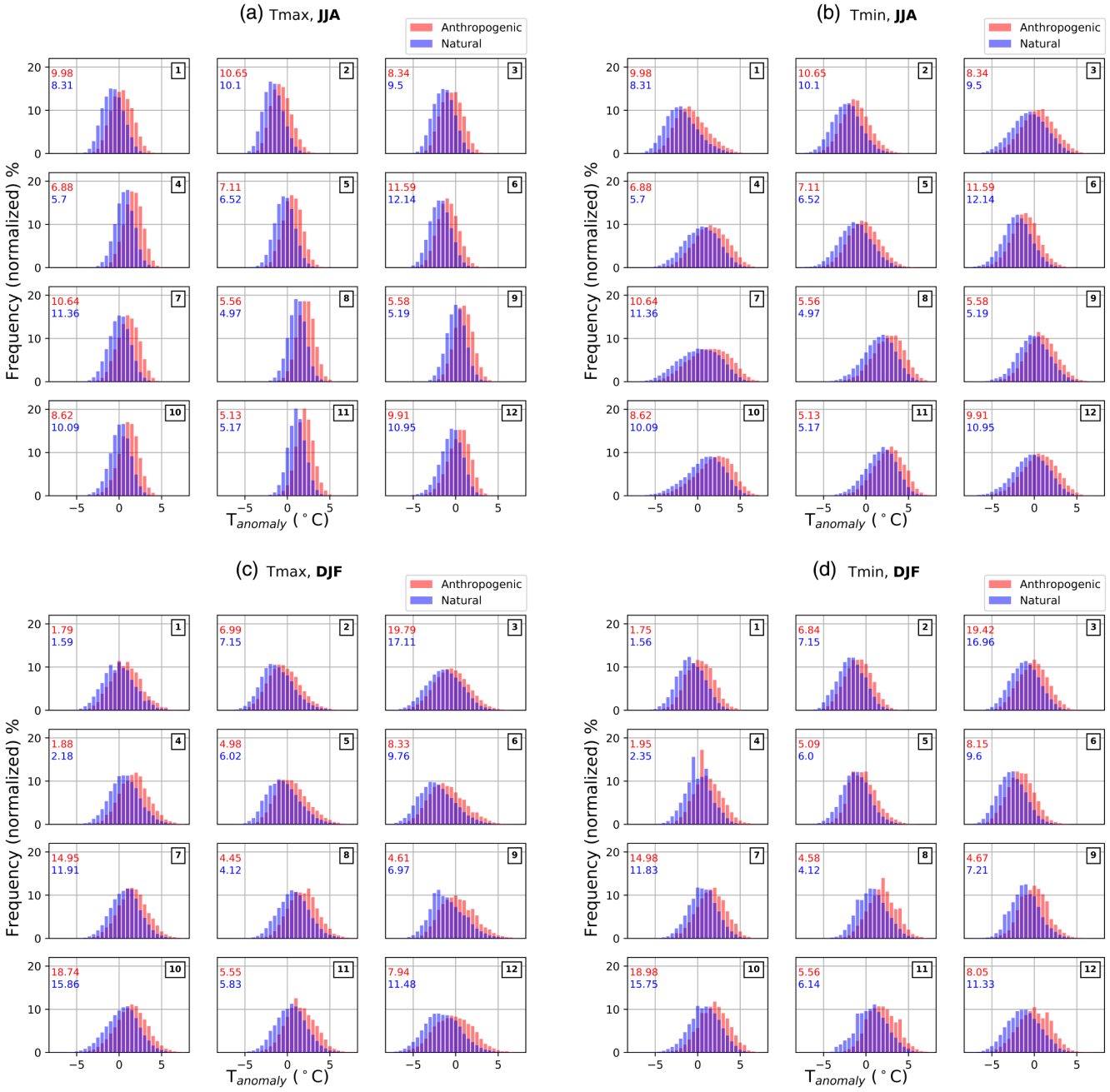

FIGURE 6 T_{max} and T_{min} anomaly probability density functions for the ANT and NAT model ensembles for JJA (a, b) and DJF (c, d) seasons over the New Zealand domain for corresponding 12 nodes (see Figure 2). The anomalies are calculated using the climatology of the respective ensembles. The number inset indicates the percentage frequency of occurrence of T_{max} and T_{min} for each node out of the total occurrences of ANT (red) and NAT (blue) ensembles. Numbers in the top right box indicate the node number [Colour figure can be viewed at wileyonlinelibrary.com]

From Figure 7, the frequency of T_{max} and T_{min} vary strongly across different circulation types and also across seasons. However, it is clear that the anthropogenic world (ANT) experiences more frequent temperatures from the ratios of ANT to NAT occurrences. The ratio varies among the nodes representing different circulation types showing at least a 1.5- to 2-fold rise in the occurrence of temperature extremes in the ANT ensemble compared to NAT (Figure 7). Certain nodes (nodes 2, 3 and 6) show more than a 7-fold rise in the frequency of extreme temperatures in the ANT compared to the NAT (Figure 7a). However, these synoptic patterns overall occur rarely. From the frequencies of occurrences associated with different circulation types, irrespective of the seasons, nodes 7 and 10 have the most frequently observed extreme temperature over

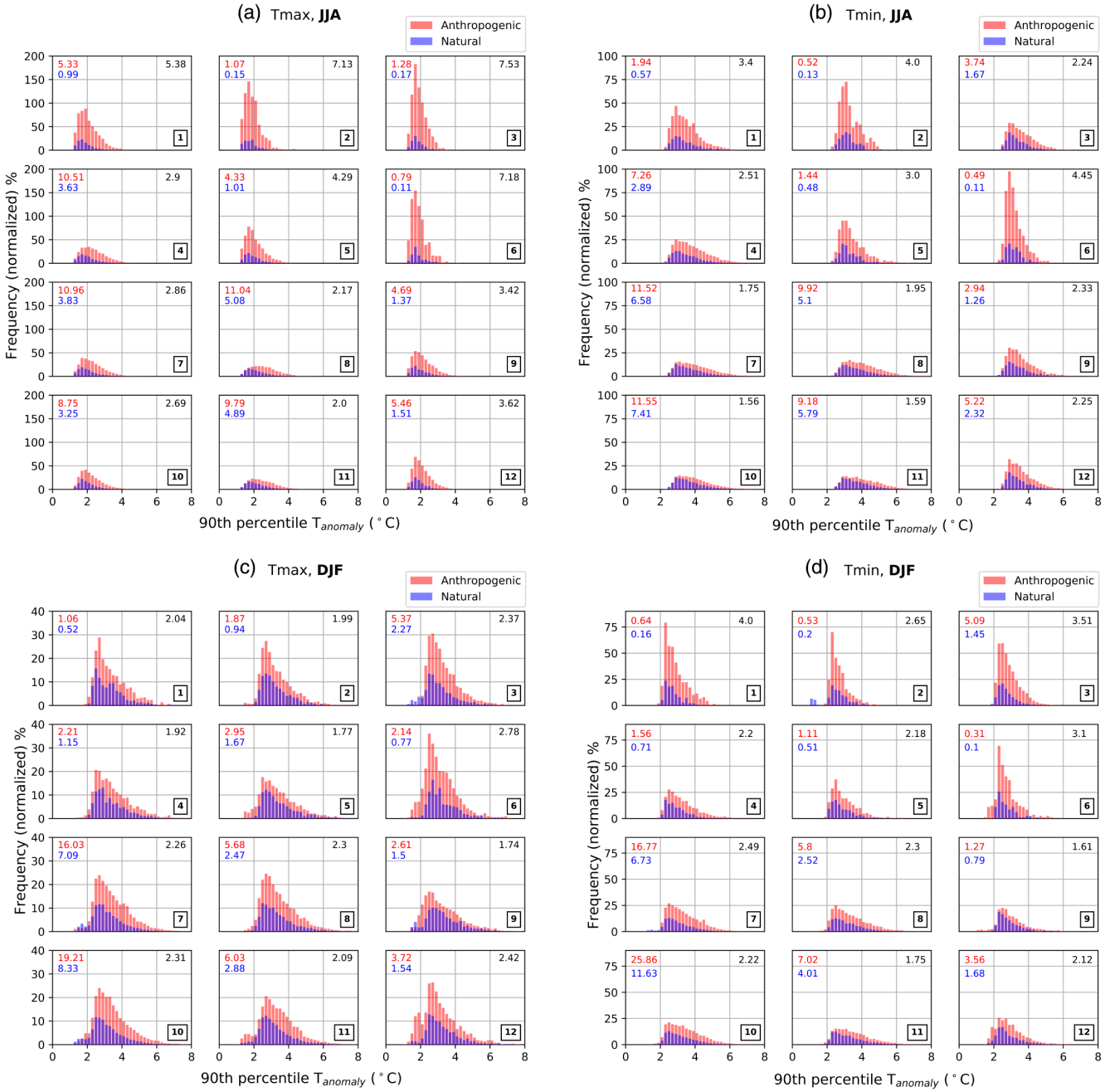

FIGURE 7 Probability distribution of 90th percentile temperature anomalies for the two model ensembles (ANT and NAT) over the NZ domain. (a, b) For winter (JJA) and (c, d) for summer (DJF) seasons. The anomalies are calculated using the climatology of the respective ensembles and the threshold used are the 90th percentile value of NAT ensemble simulations. The number inset indicates the percentage frequency of occurrence of extreme temperatures for each node out of total occurrences of ANT (red) and NAT (blue). The numbers in the top right (black) indicate the proportion of ANT to NAT occurrences (ratio). Numbers in the bottom right box indicate the node number. The NAT and ANT histograms are normalized using the NAT data. Please note that the *y*-axis for the panels are different [Colour figure can be viewed at wileyonlinelibrary.com]

New Zealand relative to the other nodes. It is noteworthy that these nodes are not associated with blocking circulation types over the landmass, which commonly produce above normal temperatures largely by subsidence of air (high surface pressure) and the associated warming and radiation leading to extreme heat (Kidson, 2000; Renwick, 2011; Marshall *et al.*, 2014). In fact these nodes (7 and 10) are associated with low-pressure centres to the north west of New Zealand, with accompanying flow that suggests that the advection of warm air from further north is an important process in the development of extreme temperature (Figure 2).

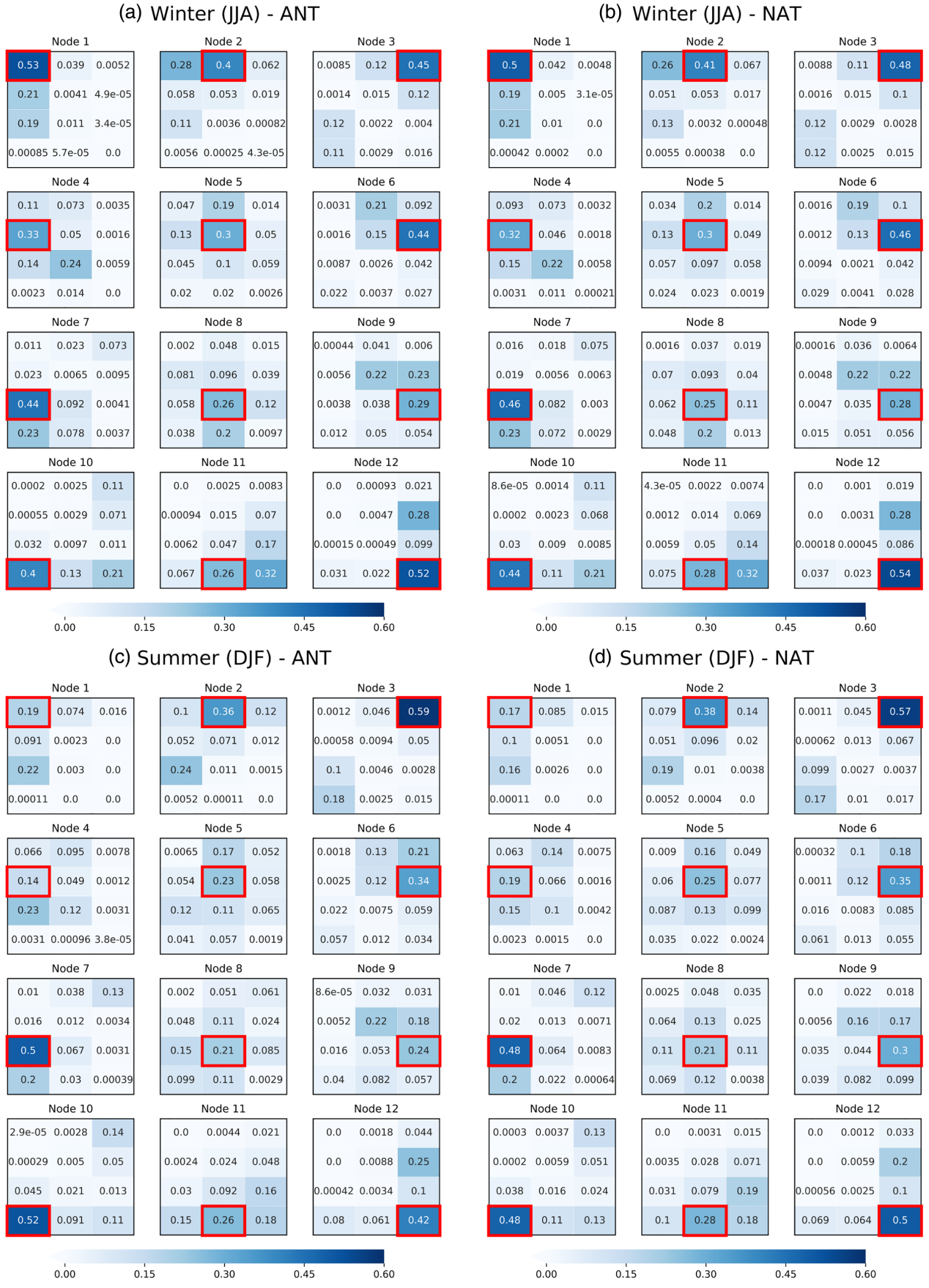

FIGURE 8 Legend on next page.

Because the persistence of synoptic situations can be an important factor in heat extremes, we examine how each of the nodes are related to each other by calculating the transition probabilities between SOM nodes. The transition probability represents the probability of moving from one node of the system to another (Figure 8). During the winter (Figure 8a,b) there is a tendency for the same synoptic state to persist in just over half of the nodes (except nodes 4, 5, 8, 9, 11) with 7 out of 12 nodes staying in the same circulation type for the next day more than 40% of the time. We also observe that in winter the occurrence of different nodes is more uniform (Figures 6 and 7) and the level of persistence is larger (Figure 8). In contrast, in the summer season (Figure 8c,d), only 4 out of 12 nodes (nodes 3, 7, 10, 12) are as persistent and instead have a tendency to transition to the neighbouring circulation patterns in the SOM. The persistent nodes tend to stay in the same synoptic state for 50% of the time compared to the other nodes which persist on average 25% of the time. There is not much notable difference between the transition probabilities of ANT and NAT as we move across the SOM nodes, thus, the individual classes have not become more persistent, that is, it is not just the individual heat events that are lasting longer. Therefore, by looking into the Sammon map (Figure 4) and the transition probabilities, it is possible to identify and then create broader clusters as also done in Kidson (2000).

3.2 | Composites

Circulation types with low pressure centres to the northwest of New Zealand (Figure 2), that is, nodes 7 and 10, are clustered together for further analysis as they are associated with days that exhibit positive temperature anomalies for T_{max} and T_{min} in New Zealand for both ANT and NAT ensembles (Figure 7). From our probability analysis of temperature anomalies and anomalies above the 90th percentiles during both summer and winter seasons (Figures 6 and 7), it can be seen that these circulation types occur more often over New Zealand than other synoptic weather patterns and that their temperatures are higher compared to most of the other circulation types. Node 7 also has the highest tendency to transit into node 10 making them excellent candidates for grouping (Figure 8). Hence it is interesting to examine how the frequency and intensity of extreme temperatures vary between the ANT and NAT scenario when analysing the synoptic circulation types of node 7 and 10 combined. We use a weighted composite of node 7 and node 10 which shows that the T_{max} and T_{min} anomalies are overall more positive in the summer season than the winter and that positive anomalies are expected more frequently in the anthropogenic simulations (Figure 9a). Looking into the extreme temperature anomalies or the 90th percentile of our PDFs it is seen that extreme T_{max} and T_{min} are more frequent in the summer seasons (Figure 9b). However, the impact of the anthropogenic influence on T_{max} is more pronounced during the winter (2.8 times than that of NAT) as observed from the ANT/NAT ratio even though extreme days occur more often in summer (Figure 9b). In the ANT simulations, the frequency of occurrence of extreme temperature in both winter and summer are up to 2.2 times on average that in the NAT. T_{min} in summer also shows a similar rise in the ANT ensemble compared to NAT but has a slightly less pronounced tendency than T_{max}.

The spatial variability of the mean T_{max} and T_{min} and extremes (temperatures above the 90th percentiles) also shows some interesting features. During winter the temperatures in Figure 10 display the highest values over the Northland region and Auckland regions in both the NAT and ANT ensembles (Figure 10a). In summer, Canterbury is also among the regions experiencing the highest temperatures (T_{max}) along with the regions in the North Island (Figure 10b). Summer T_{min} in many locations of North Island are also high (Figure 10b). It can also be observed that the seasonal variation is more prominent for T_{max} with up to 11°C, while it is 9°C for T_{min}. By examining the difference in temperatures between ANT and NAT, it is estimated that the influence of anthropogenic forcings leads to a large north–south variation in the temperatures in the ANT ensemble compared to NAT in the winter season (Figure 10a; ANT–NAT). This variation is especially enhanced in Southland, Otago and along the west coast of the South Island (Figure 10a; ANT–NAT) with difference of up to 2°C at some grid points. The summer season shows a large rise in temperature along the North Island in the ANT ensemble compared to NAT (Figure 10b; ANT–NAT) but with less north–south variation than the winter season. Across New Zealand, an average of 1°C temperature increase is observed due to anthropogenic influences in the ANT simulations for the circulation types discussed here, that is, the low-pressure centres to the northwest of New Zealand.

The 90th percentile temperature for the composite are spatially analysed to understand which regions of

FIGURE 8 Transition probabilities of the synoptic circulation types (colourbar indicating the probability). Numbers indicate the probability of each highlighted node to transit to its neighbouring nodes. Anthropogenic and natural ensembles for both the winter-JJA (a, b) and summer-DJF (c, d) season [Colour figure can be viewed at wileyonlinelibrary.com]

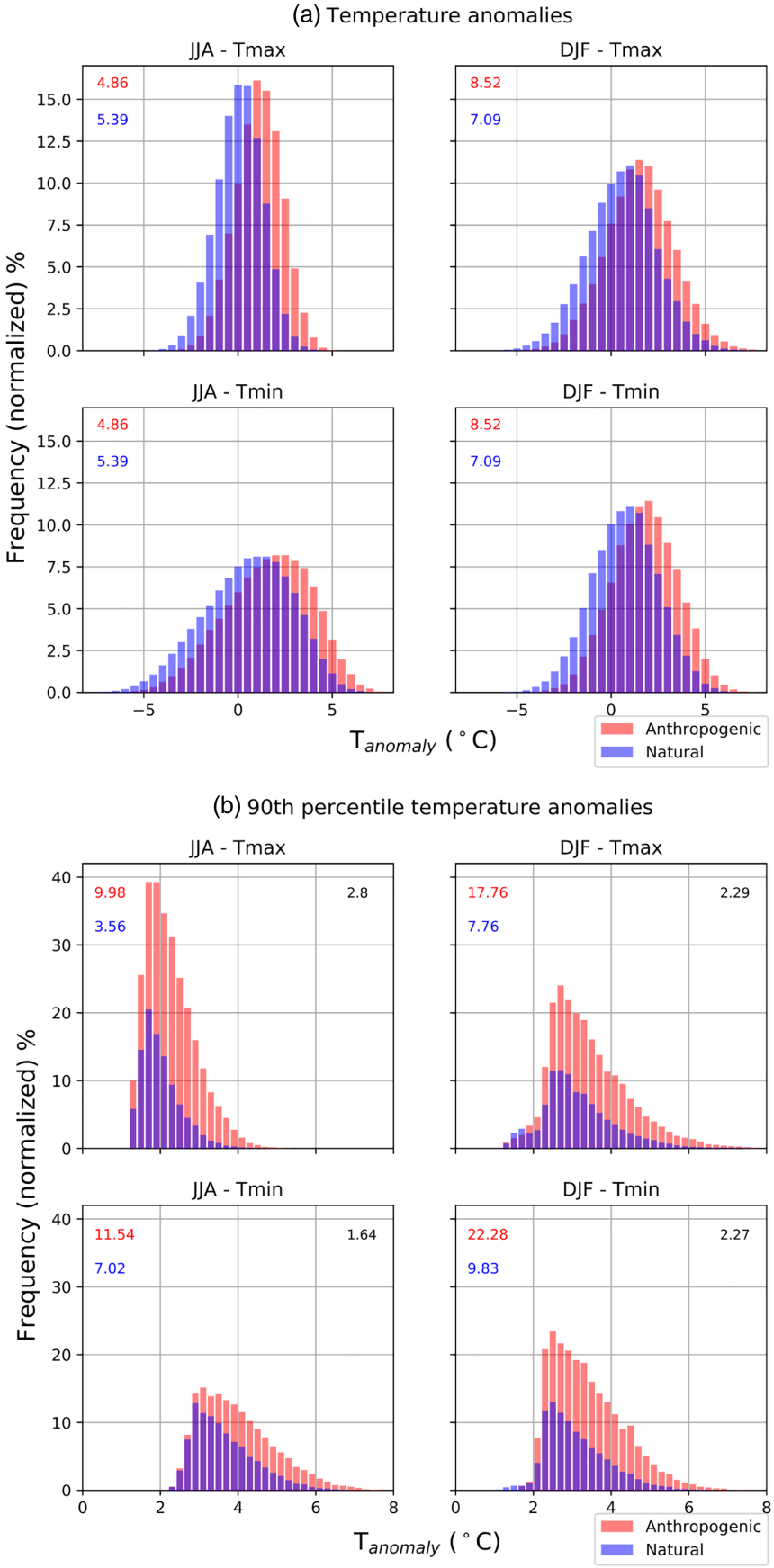

FIGURE 9 Weighted composites of nodes 7 and 10 of circulation patterns (ref Figure 2). (a) Composites of T_{max} and T_{min} anomaly and b) 90th percentile temperature anomaly distributions of the composite for the NAT and ANT model ensemble for JJA and DJF season over New Zealand domain. The number inset indicates the weighted average of nodes 7 and 10's percentage frequency of occurrence of extreme temperatures out of total occurrences of ANT (red) and NAT (blue). The numbers in the top right (black) in (b) indicate the proportion of ANT to NAT occurrences (ratio) [Colour figure can be viewed at wileyonlinelibrary.com]

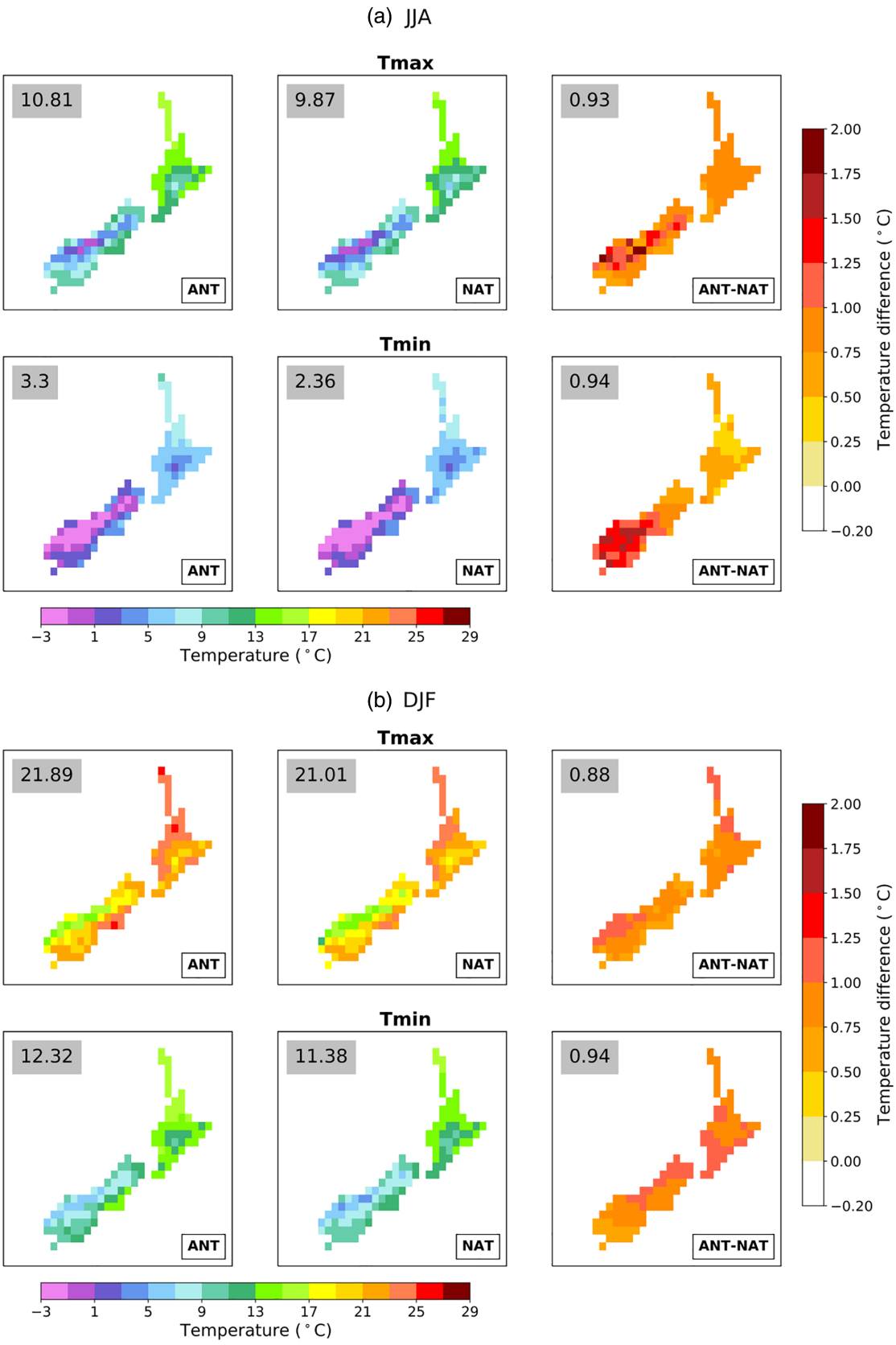

FIGURE 10 Composite spatial patterns (nodes 7 and 10) for T_{max} and T_{min} for ANT and NAT ensemble simulations and their differences at each grid point during (a) winter season (JJA) and (b) summer season (DJF). The numbers in the inset (top left) indicate the weighted average temperature [Colour figure can be viewed at wileyonlinelibrary.com]

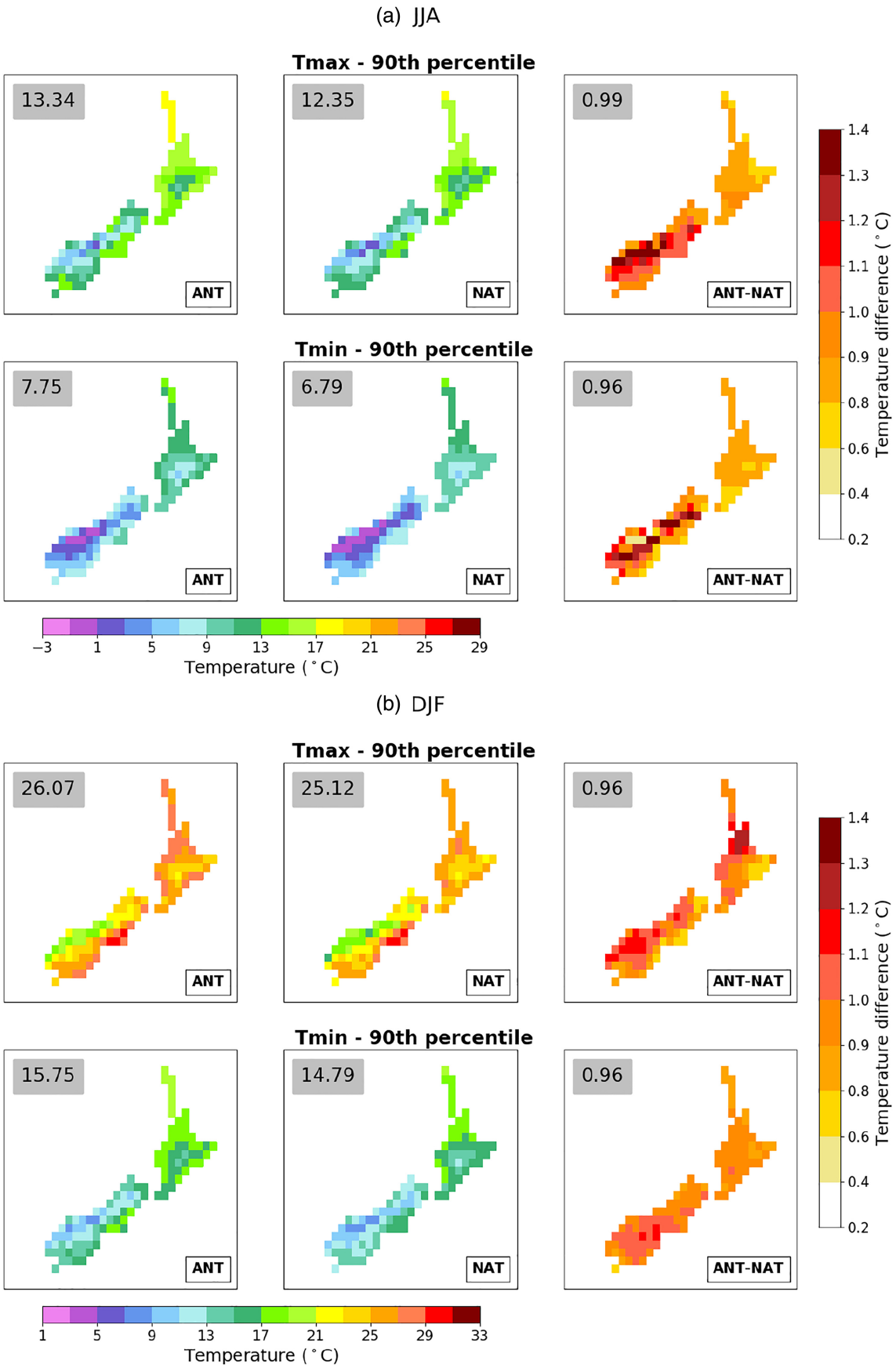

FIGURE 11 Legend on next page.

New Zealand are more prone to high temperatures (Figure 11). The 90th percentile temperatures of the composites are the weighted averaged 90th percentiles of nodes 7 and node 10 which are calculated at each grid point for the ANT and NAT ensembles, taking into account all simulation days that fall within node 7 and node 10. The spatial pattern of these highest temperatures are similar to those of the patterns for T_{max} and T_{min}, that is, they exhibit high winter-time T_{max} and T_{min} around the regions of Northland and Auckland in the upper North Island (Figure 11a). Most of the highest summer T_{max} and T_{min} extremes are observed around coastal Canterbury and Northland (Figure 11b; T_{max} and T_{min}). Extreme (90th percentile) temperatures increase on an average by 1°C in all locations within New Zealand due to anthropogenic influences as can be seen from the rightmost panels of Figure 11a,b showing ANT–NAT differences. A north–south variation is observed in winter with regions around the Southern Alps and west coast of the South Island showing the highest response to anthropogenic forcings with more than 1.4°C temperature rise compared to the NAT ensemble. Summer T_{max} shows a rise of almost 1.4°C along the Waikato regions in the North Island. A change of up to 1.2°C in the ANT ensemble is observed in certain locations, such as the west coast and parts of the South Island. In summary, evaluating how the 90th percentile of temperatures is shifting due to anthropogenic climate change for synoptic situations with a low-pressure system northwest of New Zealand shows that in winter the Southern Alps and the west coast of the South Island of New Zealand see the highest increase in their extreme temperatures, that is, the largest shift in 90th percentile threshold of T_{max} and T_{min}. Within summer, the largest increase of the 90th percentile T_{max} is visible in Waikato and otherwise a tendency to larger increases along the west coast is visible. For summer the T_{max} largely rises along the west coast of New Zealand specially over Waikato, whereas T_{min} has an overall uniform increase of 1°C across the country.

4 | DISCUSSION AND CONCLUSIONS

Gaining a better understanding of changes in the likelihood of extreme temperatures due to the effects of anthropogenic climate change is important to prepare for the related impacts. This study quantifies how anthropogenic forcing has influenced temperature extremes in New Zealand. The SOM-based approach allows us to understand under which synoptic conditions extreme temperatures are likely to become more or less frequent and by how much it varies in occurrence and intensity. The two meteorological parameters T_{max} and T_{min} are classified and clustered based on circulation patterns derived from a SOM analysis of MSLP. Our analysis suggests that particular synoptic states which favour enhanced warm air advection from further north of New Zealand appear to be important in the development of extreme high temperatures. New Zealand being an island in the open southwest Pacific Ocean, contrasting air masses from the subtropics and the Southern Ocean interact with the circulation systems to strongly control the weather.

The "weather@home" model has been widely used for temperature attribution studies, including temperature extremes, but studies over New Zealand in the literature are limited. One extreme temperature event attribution appears in Stone *et al.* (2022), finding a significant anthropogenic influence of increased temperature extremes in w@h along with other models, but the main focus of that study was to compare attribution statements across varying levels of experiment conditioning. For Australia, Black *et al.* (2015) used w@h ANZ to identify that prolonged heat extremes, similar to the 2014 Adelaide event, have increased at least by 16% due to anthropogenic influence. Similarly, research by King *et al.* (2015) showed that w@h ANZ model simulations indicated a rise of hot and extreme hot days in November by at least 25 and 44%, respectively, in Brisbane. Numerous attribution studies from different parts of the world using w@h ensembles also identify the effects of anthropogenic forcing on extreme temperature events, such as Vautard *et al.* (2020) and Undorf *et al.* (2020) for European heat events, Philip *et al.* (2018) in the United States and (Sparrow *et al.*, 2018; Van Oldenborgh *et al.*, 2018; Min *et al.*, 2020) for different regions over Asia.

A study by Dean and Stott (2009) observed that temperatures over New Zealand are higher when synoptic patterns are linked to meridional flows. The coupled ocean–atmosphere summer heatwave in New Zealand in 2017/2018 was associated with a circulation pattern with

FIGURE 11 Composite spatial patterns of 90th percentile T_{max} and T_{min} for ANT and NAT ensemble and their differences at each grid point during (a) winter season (JJA) and (b) summer season (DJF). The numbers in the inset (top left) indicate the weighted average of 90th percentile temperatures of nodes 7 and 10. Pay attention to the scales for the temperatures for JJA and DJF, as they are different [Colour figure can be viewed at wileyonlinelibrary.com]

negative pressure anomalies to the northwest of New Zealand and a northeasterly airflow anomaly was observed with it (Salinger *et al*., 2020b). The presence of an anticyclonic circulation in the northwest of New Zealand generally brings stable conditions leading to colder than average days with persistent strong south-westerly winds (Fiddes *et al*., 2016). Several studies on the synoptic climatology of glacial ablation have also identified that the advection of warm moist air from sub-tropical areas to the north, creates a strong temperature gradient leading to high ablation rates (Hay and Fitzharris, 1988; Basher and Thompson, 1996). The Brewster glacier melt in 2011 was also strongly enhanced due to warm, moist air masses advected from the northwest (Kropač *et al*., 2021). The latest study by Pohl *et al*. (2022) states that the major component of temperature variability over New Zealand is the advection of warm meridional air from low latitudes and/or cold dry air from the poles. In Figure 7 we show that the circulation type with a low-pressure centre to the northwest of New Zealand and associated poleward flow, is associated with frequent extreme temperatures over the region. This may be due to the capability of these synoptic types to advect air masses originating over warm subtropical waters with higher sea surface temperature.

From our analysis of the temperature anomaly PDFs and spatial analysis of T_{max} and T_{min} and their 90th percentiles, we highlight the following major conclusions:

1. The PDFs of T_{max} and T_{min} and their 90th percentiles show that, on average (of all the nodes), in both the summer and winter seasons, New Zealand experiences a 2.5 to 3-fold rise in the frequency of T_{max} and T_{min} compared to the NAT ensemble due to the anthropogenic forcing. In particular synoptic circulation types, changes as large as a 7 to 7.5-fold rise in T_{max} extremes are observed in the ANT ensemble compared to the NAT, though these circulation patterns occur rarely. This highlights the importance of circulation type in determining how the frequency of extreme temperatures may change due to anthropogenic influences. We also identify that the trough-like patterns show a decrease in frequency in the ANT ensemble compared to NAT as previously identified in observations by Sturman and Quénol (2013) and Jiang *et* al. (2013).
2. Out of the 12 different synoptic circulation types defined, the ones with a low-pressure centre to the northwest of New Zealand are associated with the frequent extremes. These circulation types are accompanied by meridional advection of warm air masses, which is an important determinant of extreme heat. Looking into the composites of these circulation patterns, the frequency of occurrence of T_{max} and T_{min} in the anthropogenically forced ensemble is almost 2.2 times that of the NAT for both the seasons. Seasonal variability shows that the summer season is more prone (almost double) to anthropogenic forced extreme temperatures than the winter in the composites 9.
3. The spatial variability of the temperatures shows seasonality in the composite synoptic conditions (types with a low-pressure centre to the northwest of New Zealand, that is, nodes 7 and 10). In winters the highest temperatures are observed in Northland and Auckland regions, whereas in summer, it extends from the Canterbury region through the east coast of the country to Southland along with the Northland and coastal regions in the North Island. Analysing differences caused by anthropogenic influence in the ANT and NAT ensemble, winter seasons exhibit a north–south variation with the southern part of the South Island having 1.5–2°C extra warming compared to the NAT ensemble for the T_{max} and T_{min} and almost 1.4°C variation in the extreme temperatures. In summer there is an east–west variation with an average of 1.5°C more warming in the ANT ensemble for both T_{max} and T_{min} and their extreme temperatures (90th percentiles). Overall, in association with these circulation types, the w@h ensemble simulations show that New Zealand experienced at least 1°C of temperature rise in all regions due to anthropogenic climate change. The west coast and Southern Alps region have the highest change in extreme temperatures when nodes 7 and 10 occurs.

Under an anthropogenic scenario extreme temperature anomalies are larger due to the effect of anthropogenic forcings compared to the natural pre-industrial conditions. Overall, the frequency of New Zealand temperature extremes shows at least a 2-fold rise compared to a world devoid of anthropogenic warming irrespective of the season and synoptic condition. Some synoptic patterns show a large variation in the frequency of extremes when comparing ANT and NAT ensemble simulations with up to a 7-fold rise in the winter season, however, these synoptic patterns (e.g., node 1 and 2) rarely occur. The T_{max}, T_{min} and the extremes for the composite circulations also increased by at least 1°C in all the locations of New Zealand within the anthropogenic ensemble, with higher values over the mountains of the Southern Alps, where the maximum increase is almost 2°C. Harrington (2021) also observed a similar trend in several regions, particularly over the North Island, which shows more than a doubling in the number

of hot days in the most recent decade for both November and March. Using large ensembles of simulations from the w@h model NAT and ANT datasets we observe that human influence is increasing the frequencies and intensities of extreme temperatures over New Zealand and that these variations are sensitive to synoptic circulation patterns. A better understanding of the anthropogenic contributions to the increase in extremes is important such that prompt and precise attribution statements can be made in the future.

AUTHOR CONTRIBUTIONS

Anjali Thomas: Conceptualization; data curation; formal analysis; investigation; methodology; visualization; writing – original draft preparation. **Adrian McDonald**: Conceptualization; methodology; resources; supervision; validation; visualization; writing – review & editing. **James Renwick**: Conceptualization; methodology; resources; supervision; validation; visualization; writing – review & editing. **Jordis S. Tradowsky**: Funding acquisition; project administration; resources; supervision; validation; visualization; writing – review & editing. **Greg E. Bodeker**: Funding acquisition; project administration; resources; supervision; validation; visualization; writing – review & editing. **Suzanne Rosier**: Data curation; supervision; validation; visualization; writing – review & editing.

ACKNOWLEDGEMENTS

Weather@home ANZ is a collaboration among the University of Oxford, the UK Met Office, the ARC Centre of Excellence for Climate System Science in Australia, NIWA in New Zealand, the University of Melbourne, the University of Tasmania and the Tasmanian Partnership for Advanced Computing. We thank the volunteers who donated their computing time to run weather@home. Anjali Thomas, Greg E. Bodeker and Jordis S. Tradowsky acknowledge funding from the Ministry of Business, Innovation and Employment (MBIE), New Zealand, through the EWERAM project (Contract No. BSCIF1801). Suzanne Rosier acknowledges funding support from MBIE, New Zealand, via the Deep South National Science Challenge. Open access publishing facilitated by University of Canterbury, as part of the Wiley - University of Canterbury agreement via the Council of Australian University Librarians.

CONFLICT OF INTEREST

The authors declare no potential conflict of interest.

ORCID

Anjali Thomas https://orcid.org/0000-0001-5745-0166

REFERENCES

Allen, M. (1999) Do-it-yourself climate prediction. *Nature*, 401, 642.

Amante, C. and Eakins, B.W. (2009) *Etopo1 1 arc-minute global relief model: procedures, data sources and analysis*. Boulder, CO: National Geophysical Data Center, NOAA. NOAA technical memorandum NESDIS NGDC-24, p. 10.

Basher, R.E. and Thompson, C.S. (1996) Relationship of air temperatures in New Zealand to regional anomalies in sea-surface temperature and atmospheric circulation. *International Journal of Climatology*, 16, 405–425. https://doi.org/10.1002/(SICI)1097-0088(199604)16:4<405::AID-JOC14>3.0.CO;2-T.

Bindoff, N., Stott, P., AchutaRao, K., Allen, M., Gillett, N., Gutzler, D., Hansingo, K., Hegerl, G., Hu, Y., Jain, S., Mokhov, I., Overland, J., Perlwitz, J., Sebbari, R. and Zhang, X. (2013) Detection and attribution of climate change: from global to regional. In: *Climate Change 2013: The Physical Science Basis. Contribution of Working Group I to the Fifth Assessment Report of the Intergovernmental Panel on Climate Change*. Cambridge: Cambridge University Press, pp. 867–952.

Black, M.T., Karoly, D.J. and King, A.D. (2015) The contribution of anthropogenic forcing to the Adelaide and Melbourne, Australia, heat waves of january 2014. *Bulletin of the American Meteorological Society*, 96, S145–S148.

Black, M.T., Karoly, D.J., Rosier, S.M., Dean, S.M., King, A.D., Massey, N.R., Sparrow, S.N., Bowery, A., Wallom, D., Jones, R. G., Otto, F.E.L. and Allen, M.R. (2016) The weather@home regional climate modelling project for Australia and New Zealand. *Geoscientific Model Development*, 9, 3161–3176. https://doi.org/10.5194/gmd-9-3161-2016.

Caloiero, T. (2017) Trend of monthly temperature and daily extreme temperature during 1951–2012 in New Zealand. *Theoretical and Applied Climatology*, 129, 111–127.

Dean, S. and Stott, P. (2009) The effect of local circulation variability on the detection and attribution of New Zealand temperature trends. *Journal of Climate*, 22, 6217–6229. https://doi.org/10.1175/2009JCLI2715.1.

Dee, D.P., Uppala, S.M., Simmons, A., Berrisford, P., Poli, P., Kobayashi, S., Andrae, U., Balmaseda, M., Balsamo, G., Bauer, D.P., Bechtold, P., Beljaars, A.C.M., Van de Berg, L., Bidlot, J., Bormann, N., Delsol, C., Dragani, R., Fuentes, M., Geer, A.J., Haimberger, L., Healy, S.B., Hersbach, H., Holm, E. V., Isaksen, L., Kallberg, P., Kohler, M., Matricardi, M., McNally, A.P., Monge-Sanz, B.M., Morcrette, J.-J., Park, B.-K., Peubey, C., de Rosnay, P., Tavolato, C., Thepaut, J.-N. and Vitart, F. (2011) The era-interim reanalysis: configuration and performance of the data assimilation system. *Quarterly Journal of the Royal Meteorological Society*, 137, 553–597. https://doi.org/10.1002/qj.828.

Donlon, C.J., Martin, M., Stark, J., Roberts-Jones, J., Fiedler, E. and Wimmer, W. (2012) The operational sea surface temperature and sea ice analysis (OSTIA) system. *Remote Sensing of Environment*, 116, 140–158.

Douris, J. and Kim, G. (2021) *The atlas of mortality and economic losses from weather, climate and water extremes (1970–2019)*. Geneva: World Meteorological Organization. WMO Publication No. 1267. Available at: https://library.wmo.int/doc_num.php?explnum_id=1090.

Evans, J. (2011) Cordex–an international climate downscaling initiative. In: *19th International Congress on Modelling and Simulation*. Perth: MSE-LES, pp. 12–16.

Fiddes, S., Pezza, A., Mitchell, T., Kozyniak, K. and Mills, D. (2016) Synoptic weather evolution and climate drivers as sociated with winter air pollution in New Zealand. *Atmospheric Pollution Research*, 7, 1082–1089. https://doi.org/10.1016/j.apr.2016.06.014.

Fischer, E.M. and Knutti, R. (2015) Anthropogenic contribution to global occurrence of heavy-precipitation and high temperature extremes. *Nature Climate Change*, 5, 560–564. https://doi.org/10.1038/nclimate2617.

Folland, C.K. and Salinger, M.J. (1995) Surface temperature trends and variations in New Zealand and the surrounding ocean, 1871–1993. *International Journal of Climatology*, 15, 1195–1218.

Frame, D.J., Rosier, S.M., Noy, I., Harrington, L.J., Carey-Smith, T., Sparrow, S.N., Stone, D.A. and Dean, S.M. (2020) Climate change attribution and the economic costs of extreme weather events: a study on damages from extreme rainfall and drought. *Climatic Change*, 162, 781–797.

Gibson, P.B., Uotila, P., Perkins-Kirkpatrick, S.E., Alexander, L.V. and Pitman, A.J. (2016) Evaluating synoptic systems in the CMIP5 climate models over the australian region. *Climate Dynamics*, 47, 2235–2251. https://doi.org/10.1007/s00382-015-2961-y.

Gordon, C., Cooper, C., Senior, C.A., Banks, H., Gregory, J.M., Johns, T.C., Mitchell, J.F. and Wood, R.A. (2000) The simulation of sst, sea ice extents and ocean heat transports in a version of the hadley centre coupled model without flux adjustments. *Climate Dynamics*, 16, 147–168.

Harrington, L.J. (2021) Rethinking extreme heat in a cool climate: a New Zealand case study. *Environmental Research Letters*, 16, 034030. https://doi.org/10.1088/1748-9326/abbd61.

Harrington, L.J., Rosier, S., Dean, S.M., Stuart, S. and Scahill, A. (2014) The role of anthropogenic climate change in the 2013 drought over north Island, New Zealand. *Bulletin of the American Meteorological Society*, 95, S45–S48.

Hay, J. and Fitzharris, B. (1988) The synoptic climatology of ablation on a New Zealand glacier. *Journal of Climatology*, 8, 201–215. https://doi.org/10.1002/joc.3370080207.

Hegerl, G., Zwiers, F.W., Braconnot, P., Gillett, N., Luo, Y., Orsini, J.M., Nicholls, N., Penner, J. and Stott, P. (2007) Understanding and attributing climate change. In: *Climate Change 2007: The Physical Science Basis. Contribution of Working Group I to the Fourth Assessment Report of the Intergovernmental Panel on Climate Change*. Cambridge and New York, NY: Cambridge University Press, pp. 663–745.

Hersbach, H., Bell, B., Berrisford, P., Hirahara, S., Horányi, A., Muñoz-Sabater, J., Nicolas, J., Peubey, C., Radu, R., Schepers, D., Simmons, A., Soci, C., Abdalla, S., Abellan, X., Balsamo, G., Bechtold, P., Biavati, G., Bidlot, J., Bonavita, M., Chiara, G., Dahlgren, P., Dee, D., Diamantakis, M., Dragani, R., Flemming, J., Forbes, R., Fuentes, M., Geer, A., Haimberger, L., Healy, S., Hogan, R.J., Hólm, E., Janisková, M., Keeley, S., Laloyaux, P., Lopez, P., Lupu, C., Radnoti, G., Rosnay, P., Rozum, I., Vamborg, F., Villaume, S. and Thépaut, J.N. (2020) The ERA5 global reanalysis. *Quarterly Journal of the Royal Meteorological Society*, 146, 1999–2049. https://doi.org/10.1002/qj.3803.

Hewitson, B.C. and Crane, R.G. (2002) Self-organizing maps: applications to synoptic climatology. *Climate Research*, 22, 13–26. https://doi.org/10.3354/cr022013.

Horton, D.E., Johnson, N.C., Singh, D., Swain, D.L., Rajaratnam, B. and Diffenbaugh, N.S. (2015) Contribution of changes in atmospheric circulation patterns to extreme temperature trends. *Nature*, 522, 465–469. https://doi.org/10.1038/nature14550.

Horton, R.M., Mankin, J.S., Lesk, C., Coffel, E. and Raymond, C. (2016) A review of recent advances in research on extreme heat events. *Current Climate Change Reports*, 2, 242–259. https://doi.org/10.1007/s40641-016-0042-x.

Jiang, N. (2011) A new objective procedure for classifying New Zealand synoptic weather types during 1958–2008. *International Journal of Climatology*, 31, 863–879.

Jiang, N., Griffiths, G. and Lorrey, A. (2013) Influence of large scale climate modes on daily synoptic weather types over New Zealand. *International Journal of Climatology*, 33, 499–519. https://doi.org/10.1002/joc.3443.

Jones, R., Noguer, M., Hassell, D., Wilson, S., Jenkins, G. and Mitchell, J. (2004) *Generating high resolution climate change scenarios using precis*. Technical report.

Kidson, J.W. (2000) An analysis of New Zealand synoptic types and their use in defining weather regimes. *International Journal of Climatology*, 20, 299–316.

King, A.D., Black, M.T., Karoly, D.J. and Donat, M.G. (2015) Increased likelihood of Brisbane, Australia, G20 heat event due to anthropogenic climate change. *Bulletin of the American Meteorological Society*, 96, S141–S144.

Kohonen, T. (2001) Self-organizing maps. In: *Information Sciences*. Berlin: Springer, p. 30.

Kropač, E., Mölg, T., Cullen, N.J., Collier, E., Pickler, C. and Turton, J.V. (2021) A detailed, multi-scale assessment of an atmospheric river event and its impact on extreme glacier melt in the southern alps of New Zealand. *Journal of Geophysical Research: Atmospheres*, 126, e2020JD034217. https://doi.org/10.1029/2020JD034217.

Loikith, P.C., Lintner, B.R. and Sweeney, A. (2017) Characterizing large-scale meteorological patterns and associated temperature and precipitation extremes over the northwestern United States using self-organizing maps. *Journal of Climate*, 30, 2829–2847. https://doi.org/10.1175/JCLI-D-16-0670.1.

Manton, M.J., Della-Marta, P.M., Haylock, M.R., Hennessy, K., Nicholls, N., Chambers, L., Collins, D., Daw, G., Finet, A., Gunawan, D., Inape, K., Isobe, H., Kestin, T.S., Lefale, P., Leyu, C.H., Lwin, T., Maitrepierre, L., Ouprasitwong, N., Page, C.M., Pahalad, J., Plummer, N., Salinger, M.J., Suppiah, R., Tran, V. L., Trewin, B., Tibig, I. and Yee, D. (2001) Trends in extreme daily rainfall and temperature in southeast asia and the south pacific: 1961–1998. *International Journal of Climatology*, 21, 269–284.

Marshall, A., Hudson, D., Wheeler, M., Alves, O., Hendon, H., Pook, M. and Risbey, J. (2014) Intra-seasonal drivers of extreme heat over Australia in observations and POAMA-2. *Climate Dynamics*, 43, 1915–1937. https://doi.org/10.1007/s00382-013-2016-1.

Mason, S., Fletcher, J.K., Haynes, J.M., Franklin, C., Protat, A. and Jakob, C. (2015) A hybrid cloud regime methodology used to evaluate southern ocean cloud and shortwave radiation errors in access. *Journal of Climate*, 28, 6001–6018.

Massey, N., Jones, R., Otto, F., Aina, T., Wilson, S., Murphy, J., Hassell, D., Yamazaki, Y. and Allen, M. (2015) weather@home—development and validation of a very large ensemble

modelling system for probabilistic event attribution. *Quarterly Journal of the Royal Meteorological Society*, 141, 1528–1545. https://doi.org/10.1002/qj.2455.

Masson-Delmotte, V., Zhai, P., Pirani, A., Connors, S., Péan, C., Berger, S., Caud, N., Chen, Y., Goldfarb, L., Gomis, M., Huang, M., Leitzell, K., Lonnoy, E., Matthews, J., Maycock, T., Waterfield, T., Yelekçi, O. and Yu, R. (2021) *Climate Change 2021: The Physical Science Basis. Contribution of Working Group I to the Sixth Assessment Report of the Intergovernmental Panel on Climate Change*. Cambridge and New York, NY: Cambridge University Press. https://doi.org/10.1017/9781009157896.

Masson-Delmotte, V., Zhai, P., Pörtner, H., Roberts, D., Skea, J., Shukla, P., Pirani, A., Moufouma-Okia, W., Péan, C., Pidcock, R., Connors, S., Robin Matthews, J.B., Chen, Y., Zhou, X., Gomis, M.I., Lonnoy, E., Maycock, T., Tignor, M. and Waterfield, T. (2018) *Global Warming of 1.5°C. An IPCC Special Report on the Impacts of Global Warming of 1.5°C above Preindustrial Levels and Related Global Greenhouse Gas Emission Pathways, in the Context of Strengthening the Global Response to the Threat of Climate Change, Sustainable Development, and Efforts to Eradicate Poverty*. Cambridge and New York, NY: Cambridge University Press. https://doi.org/10.1017/9781009157940.

McDonald, A. and Parsons, S. (2018) A comparison of cloud classification methodologies: differences between cloud and dynamical regimes. *Journal of Geophysical Research: Atmospheres*, 123, 11173–11193.

McDonald, A.J., Cassano, J.J., Jolly, B., Parsons, S. and Schuddeboom, A. (2016) An automated satellite cloud classification scheme using self-organizing maps: alternative isccp weather states. *Journal of Geophysical Research: Atmospheres*, 121, 13009–13030. https://doi.org/10.1002/2016JD025199.

Min, S.-K., Kim, Y.-H., Lee, S.-M., Sparrow, S., Li, S., Lott, F.C. and Stott, P.A. (2020) Quantifying human impact on the 2018 summer longest heat wave in South Korea. *Bulletin of the American Meteorological Society*, 101, S103–S108.

Mullan, A.B. (2012) Applying the rhoades and salinger method to New Zealand's "seven-station" temperature series. *Weather and Climate*, 32, 23–37.

Parsons, S., McDonald, A.J. and Renwick, J.A. (2014) The use of synoptic climatology with general circulation model output over New Zealand. *International Journal of Climatology*, 34, 3426–3439.

Perkins, S.E. (2015) A review on the scientific understanding of heatwaves—their measurement, driving mechanisms, and changes at the global scale. *Atmospheric Research*, 164, 242–267. https://doi.org/10.1016/j.atmosres.2015.05.014.

Philip, S.Y., Kew, S.F., Hauser, M., Guillod, B.P., Teuling, A.J., Whan, K., Uhe, P. and Oldenborgh, G.J. (2018) Western us high june 2015 temperatures and their relation to global warming and soil moisture. *Climate Dynamics*, 50, 2587–2601.

Philip, S.Y., Kew, S.F., van Oldenborgh, G.J., Anslow, F.S., Seneviratne, S.I., Vautard, R., Coumou, D., Ebi, K.L., Arrighi, J., Singh, R., van Aalst, M., Pereira Marghidan, C., Wehner, M., Yang, W., Li, S., Schumacher, D.L., Hauser, M., Bonnet, R., Luu, L.N., Lehner, F., Gillett, N., Tradowsky, J., Vecchi, G.A., Rodell, C., Stull, R.B., Howard, R. and Otto, F.E. L. (2021) Rapid attribution analysis of the extraordinary heatwave on the Pacific coast of the US and Canada June 2021. *Earth System Dynamics Discussions*, 2021, 1–34.

Pohl, B., Sturman, A., Renwick, J., Quénol, H., Fauchereau, N., Lorrey, A. and Pergaud, J. (2022) Precipitation and temperature anomalies over aotearoa New Zealand analysed by weather types and descriptors of atmospheric centres of action. *International Journal of Climatology*, 2022, 1–23. https://doi.org/10.1002/joc.7762.

Pope, V., Gallani, M., Rowntree, P. and Stratton, R. (2000) The impact of new physical parametrizations in the hadley centre climate model: Hadam3. *Climate Dynamics*, 16, 123–146.

Prince, H.D., Cullen, N.J., Gibson, P.B., Conway, J. and Kingston, D.G. (2021) A climatology of atmospheric rivers in New Zealand. *Journal of Climate*, 34, 4383–4402. https://doi.org/10.1175/JCLI-D-20-0664.1.

Renwick, J.A. (2011) Kidson's synoptic weather types and surface climate variability over New Zealand. *Weather and Climate*, 31, 3–23. https://doi.org/10.2307/26169715.

Salinger, M., Allan, R., Bindoff, N., Hannah, J., Lavery, B., Lin, Z., Lindesay, J., Nicholls, N., Plummer, N. and Torok, S. (1996) Observed variability and change in climate and sea level in Australia, New Zealand and the South Pacific. In: Bouma, W.J., Pearman, G.I. and Manning, M.R. (Eds.) *Greenhouse-Coping with Climate Change*. Collingwood, Vic: CSIRO.

Salinger, M., Diamond, H. and Renwick, J. (2020a) Surface temperature trends and variability in New Zealand and surrounding oceans. *Weather and Climate*, 40, 32–51.

Salinger, M. and Griffiths, G. (2001) Trends in New Zealand daily temperature and rainfall extremes. *International Journal of Climatology: A Journal of the Royal Meteorological Society*, 21, 1437–1452.

Salinger, M. and Mullan, A. (1999) New Zealand climate: temperature and precipitation variations and their links with atmospheric circulation 1930–1994. *International Journal of Climatology*, 19, 1049–1071.

Salinger, M.J., Diamond, H.J., Behrens, E., Fernandez, D., Fitzharris, B.B., Herold, N., Johnstone, P., Kerckhoffs, H., Mullan, A.B., Parker, A.K., Renwick, J., Scofield, C., Siano, A., Smith, R.O., South, P.M., Sutton, P.J., Teixeira, E., Thomsen, M. S. and Trought, M.C.T. (2020b) Unparalleled coupled ocean-atmosphere summer heatwaves in the New Zealand region: drivers, mechanisms and impacts. *Climatic Change*, 162, 485–506. https://doi.org/10.1007/s10584-020-02730-5.

Sammon, J.W. (1969) A nonlinear mapping for data structure analysis. *IEEE Transactions on Computers*, 100, 401–409.

Sparrow, S., Su, Q., Tian, F., Li, S., Chen, Y., Chen, W., Luo, F., Freychet, N., Lott, F.C., Dong, B., Tett, S.F.B. and Wallom, D. (2018) Attributing human influence on the July 2017 Chinese heatwave: the influence of sea-surface temperatures. *Environmental Research Letters*, 13, 114004.

Stone, D.A., Rosier, S.M., Bird, L., Harrington, L.J., Rana, S., Stuart, S. and Dean, S.M. (2022) The effect of experiment conditioning on estimates of human influence on extreme weather. *Weather and Climate Extremes*, 36, 100427.

Stone, D.A., Rosier, S.M. and Frame, D.J. (2021) The question of life, the universe and event attribution. *Nature Climate Change*, 11, 276–278.

Sturman, A. and Quénol, H. (2013) Changes in atmospheric circulation and temperature trends in major vineyard regions of New Zealand. *International Journal of Climatology*, 33, 2609–2621. https://doi.org/10.1002/joc.3608.

Taylor, K.E., Stouffer, R.J. and Meehl, G.A. (2012) An overview of CMIP5 and the experiment design. *Bulletin of the American Meteorological Society*, 93, 485–498.

Tradowsky, J.S., Bird, L., Kreft, P.V., Rosier, S.M., Soltanzadeh, I., Stone, D.A. and Bodeker, G.E. (2022) Towards near realtime attribution of extreme weather events in aotearoa New Zealand. *Bulletin of the American Meteorological Society.*, 103, S105–S110.

Trenberth, K.E. (1976) Fluctuations and trends in indices of the southern hemispheric circulation. *Quarterly Journal of the Royal Meteorological Society*, 102, 65–75. https://doi.org/10.1002/qj.49710243106.

Undorf, S., Allen, K., Hagg, J., Li, S., Lott, F., Metzger, M.J., Sparrow, S. and Tett, S. (2020) Learning from the 2018 heat wave in the context of climate change: are high-temperature extremes important for adaptation in Scotland? *Environmental Research Letters*, 15, 034051.

Van Oldenborgh, G.J., Philip, S., Kew, S., van Weele, M., Uhe, P., Otto, F., Singh, R., Pai, I., Cullen, H. and AchutaRao, K. (2018) Extreme heat in India and anthropogenic climate change. *Natural Hazards and Earth System Sciences*, 18, 365–381.

Vautard, R., van Aalst, M., Boucher, O., Drouin, A., Haustein, K., Kreienkamp, F., Van Oldenborgh, G.J., Otto, F.E., Ribes, A., Robin, Y., Schneider, M., Soubeyroux, J.-M., Stott, P., Seneviratne, S.I., Vogel, M.M. and Wehner, M. (2020) Human contribution to the record breaking June and July 2019 heatwaves in western Europe. *Environmental Research Letters*, 15, 094077.

Zhang, X., Alexander, L., Hegerl, G.C., Jones, P., Tank, A.K., Peterson, T.C., Trewin, B. and Zwiers, F.W. (2011) Indices for monitoring changes in extremes based on daily temperature and precipitation data. *Wiley Interdisciplinary Reviews: Climate Change*, 2, 851–870. https://doi.org/10.1002/wcc.147.

How to cite this article: Thomas, A., McDonald, A., Renwick, J., Tradowsky, J. S., Bodeker, G. E., & Rosier, S. (2023). Increasing temperature extremes in New Zealand and their connection to synoptic circulation features. *International Journal of Climatology*, *43*(3), 1251–1272. https://doi.org/10.1002/joc.7908